CYLINDRICAL NEAR-TO-FAR-FIELD TRANSFORMATION SYSTEM FOR RADAR ANTENNAS: DESIGN, VALIDATION, AND APPLICATION

S. Burgos, F. Martín, M. Sierra-Castañer, and J. L. Besada
Radiation Group, Department of Signals, Systems and Radio Communications, Technical University of Madrid (Universidad Politécnica de Madrid, UPM), Madrid, Spain; Corresponding author: sarab@gr.ssr.upm.es
INDRA Sistemas S.A., Torrejón de Ardoz. Madrid, Spain

ABSTRACT: *Cylindrical near-field systems are appropriate measurement systems for large L-band RADAR antennas, because they can be measured on their azimuthal positioner, and the probe can be easily translated through a vertical linear slide. Thus, for large antennas, the mechanical aspects of the measurement systems are important and the errors in this mechanical part can affect to the far-field radiation pattern. This work presents the design and validation process of the near-to-far-field transformation algorithm applied to an outdoor L-band RADAR antenna cylindrical system.*

Key words: *large antennas; outdoor cylindrical near-field measurement system; antenna far-field radiation pattern; validation; intercomparisons*

DOI 10.1002/mop.

1. INTRODUCTION

Large antennas need special measurement system due to their considerable dimensions. cylindrical near-field antenna measurement systems are appropriate for this kind of RADAR antenna characterization. This study will deal with the design and validation of a near-to-far-field (NF-FF) transformation algorithm for large L-band RADAR antennas performed for a cylindrical outdoor measurement system.

The implementation selected to achieve the NF-FF transformation can be based on different approaches. In 1978, Borgiotti presented an integral formulation using a superposition of plane waves to obtain the far field from the measured near field. Later, in the works published by Hansen Yaghjian , and (the "Handbook of Antenna Design," 1982) a second methodology was detailed. In this case, the scattering matrix formulation is used to derive the coupling equation.

A third approach, introduced by Brown and Jull and Leach and Paris , is based on the three-dimensional vector cylindrical wave expansion of an electromagnetic field, which applies the Lorentz reciprocity theorem formulation to attain the complete vector far-field pattern of an arbitrary antenna. In addition to the procedure proposed by Leach, Bucci and Rahmatt-Samii studied some improvements in the efficiency of this method. In the last years, some approaches to solve the problem of near to far-field transformation using equivalent currents have been presented

This article is divided in the following sections. First, section 2 details the NF-FF transformation software implemented and its validation—through simulations and intercomparisons—is illustrated in section 3. Then, section 4 presents the system application, and last, the final conclusions are drawn in section 5.

2. NF-FF TRANSFORMATION ALGORITHM

The cylindrical near-to-far-field (NF-FF) transformation algorithm developed for this application uses the methodology based on

cylindrical wave expansion proposes by Leach . However, there are several modifications respect to that method, mainly in the probe compensation technique. The model developed for this application introduces the probe compensation implementation proposed by Hansen and normally applied for the spherical NF-FF transformation algorithms. The simulator calculates the probe pattern from the main planes of the probe diagram, and it is valid for rotationally symmetrical antenna probes ($\mu = \pm 1$). In this case, the antenna probe is a chock horn that fulfils the previous condition.

Several angular rotations of the probe radiation pattern, using the method proposed are required for being able to obtain the probe compensated far-field-radiated pattern. Another minor difference with respect to Leach's method is the employment of the discrete Fourier transform instead of the fast Fourier transform. The purpose of this change is the possibility of obtaining the far field in the final coordinate system, without the need of an interpolation of the radiation pattern results. Therefore, the NF-FF algorithm is based on the establishment of the cylindrical wave expansion $\bar{M}^{(4)}_{n\gamma}(\bar{r})$ and $\bar{N}^{(4)}_{n\gamma}(\bar{r})$, which can be expressed as follows:

$$\vec{M}^{(4)}_{nh}(\bar{r}) = \left(\left(\frac{jn}{\rho} \right) H^{(2)}_n(\kappa\rho)\hat{\rho} - \frac{\partial H^{(2)}_n(\kappa\rho)}{\partial\rho}\hat{\phi} \right) e^{jn\phi}e^{-jhz} \quad (1)$$

$$\vec{N}^{(4)}_{nh}(\bar{r}) = \left(\begin{array}{c} -\dfrac{jh\partial H^{(2)}_n(\kappa\rho)}{k \quad \partial\rho}\hat{\rho} + \dfrac{nh}{k\rho}H^{(2)}_n(\kappa\rho)\hat{\phi} + \\ + \dfrac{\kappa^2}{k}H^{(2)}_n(\kappa\rho)\hat{z} \end{array} \right) e^{jn\phi}e^{-jhz} \quad (2)$$

where $\bar{r}$ corresponds to the positioning vector of each point where the field is observed, n indicates the modal index (whole number), h symbolizes the propagation constant in the z-direction (real number) $h = k \cos\theta$, k characterizes the wave number in free space, $\kappa = \sqrt{(k^2 - h^2)} = k \sin\theta$ is the projection of the propagation constant in the xy-plane, and $H|^{(2)}_n(k\rho)$ denotes the cylindrical Hankel function of second kind and order n.

The modes $\bar{M}^{(4)}_{nh}(\bar{r})$ and $\bar{N}^{(4)}_{nh}(\bar{r})$, which are continuous in h and discrete in n, represents each orthogonal polarization, the first as a TE-mode and the second as a TM-mode, respect to the z-direction. In this way, the general expression of the radiated electric field is expressed as a linear combination of the previous functions, multiplied by the weighting functions $a_n(h)$ and $b_n(h)$:

$$\vec{E}(\bar{r}) = \sum_{n=-\infty}^{\infty} \int_{-\infty}^{\infty} \{a_n(h)\vec{M}^{(4)}_{nh}(\bar{r}) + b_n(h)\vec{N}^{(4)}_{nh}(\bar{r})\}dh \quad (3)$$

Then, the far field can be obtained directly through the infinite approach of the previous equation:

$$\vec{E}(\bar{r}) = \frac{-2\,k\sin\theta e^{-\mathrm{jkr}}}{\mathrm{r}} \sum_{\mathrm{n}=-\infty}^{\infty} j^n e^{jn\phi}(\hat{\phi}a_n(k\cos\theta) + \hat{\theta}jb_n(k\cos\theta)) \quad (4)$$

If the antenna probe is considered, the expression (3) must be modified to consider its effect on the received field. The received field by the probe can also be expressed as the next cylindrical wave expression on its coordinate system:

$$\vec{E}_b(\vec{r}') = c_m(\eta)\vec{M}^{(4)}_{m\eta}(\vec{r}') + d_m(\eta)\vec{N}^{(4)}_{m\eta}(\vec{r}') \quad (5)$$

Therefore, and using the reciprocity theorem, the electric field can be expressed as a combination of the four weighting functions [for the antenna under test (AUT) and the probe], obtaining the expression proposed by Leach

$$v(\rho_o,\phi_o,z_o) = \frac{\kappa^2}{4\pi^2k^2}\sum_{n=-\infty}^{\infty} e^{jn\phi 0}\ldots$$

$$\int_{-\infty}^{\infty}\left(a_n(h)\sum_{m=-\infty}^{\infty} c_m(-h)H^{(2)}_{n+m}(\kappa\rho_o) + b_n(h)\sum_{m=-\infty}^{\infty} d_m(-h)H^{(2)}_{n+m} \times (\kappa\rho_o)\right)\ldots e^{-jhz_o}dh \quad (6)$$

The probe coefficients can be achieved using the far field expression (3) and for rotationally symmetrical antenna probes it is enough with the acquisition of the copolar field in the main planes

A chart of the algorithm is shown in Figure 1.

3. VALIDATION PROCEDURE

The previous algorithm has been validated using both simulations and measurements. In the case of simulations, the procedure starts with the modeling of the transmitting and receiving antenna. Several simulations with different AUT models have been performed here. The AUT considered in this study is modeled as an array of 28 × 16 half-wavelength dipoles vertically displaced, over a ground plane at a distance equal to λ/4, and assumed to be infinite, and so image theory can be applied. The excitation is separable in vertical and horizontal planes and with decreasing amplitude to reduce the side lobe levels (SLLs). In the horizontal plane, a phase error is added to simulate a more realistic AUT (with higher side lobes). The total size of the simulated AUT is 5.3 m × 2.1 m.

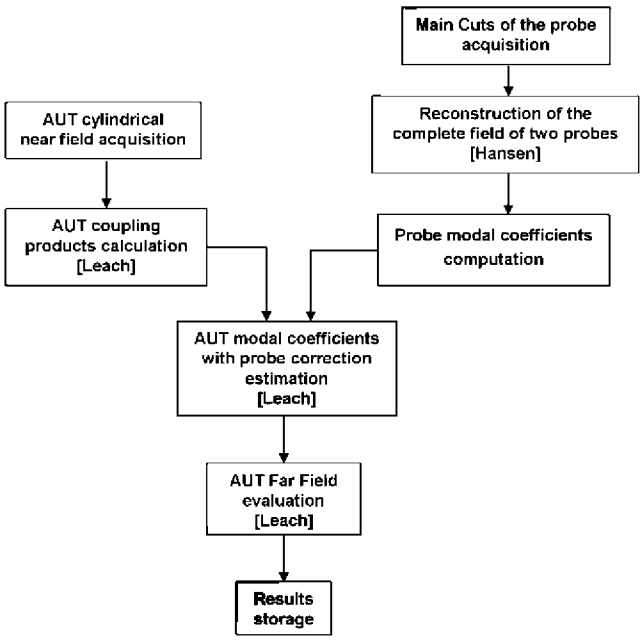

Figure 1 Diagram of NF-FF algorithm

On the other hand, the antenna probe is an ideal conical corrugated horn, and its main planes radiated field are obtained through the integration of the electric field on the aperture:

$$\vec{E}_{ap} = \hat{y} J_0\left(\frac{2.405 r'}{a}\right) e^{-j\pi r'^2/\lambda L} \tag{7}$$

The acquisition is simulated on a cylinder where the distance from the AUT to the probe tower is 5 m and the vertical path of the probe is 15 m. The number of samples in the azimuth is 256 (to satisfy the Nyquist sampling theorem), whereas the distance between samples in the vertical axis is 10 centimeters. The frequency selected for the simulations is 1215 MHz. The received field in each point of the grid was calculated taking into account the field radiated by all the dipoles modified by the probe pattern. As each element of the array could be considered in far-field respect of the antenna probe, the field from each dipole in each point of the grid is given by the sum of three spherical waves, in a similar way as explained in [16], using the following approximation:

$$E_z \approx I_{mn}\left(\frac{e^{-jkR_1}}{R_1} f_s(\theta_1) + \frac{e^{-jkR_2}}{R_2} f_s(\theta_2) - 2\cos(kL_1)\frac{e^{-jkr}}{r} f_s(\theta)\right) \tag{8}$$

where I_{mn} is the dipole excitation, the angles and distances are shown in Figure 2, and $f_s(\theta)$ is the far-field radiation pattern of the probe.

Then, the NF-FF transformation is applied to obtain the far-field radiation patterns. The results in the main planes are compared with the infinite far field obtained by multiplying the array factor by the element radiation pattern, as shown in Figures 3 and 4. Both diagrams show a great concordance between both calculated patterns, and so the NF-FF transformation could be considered validated. The small discrepancies in the extremes of the horizontal angular range are due to the approximation of the acquisition model, shown in expression (8).

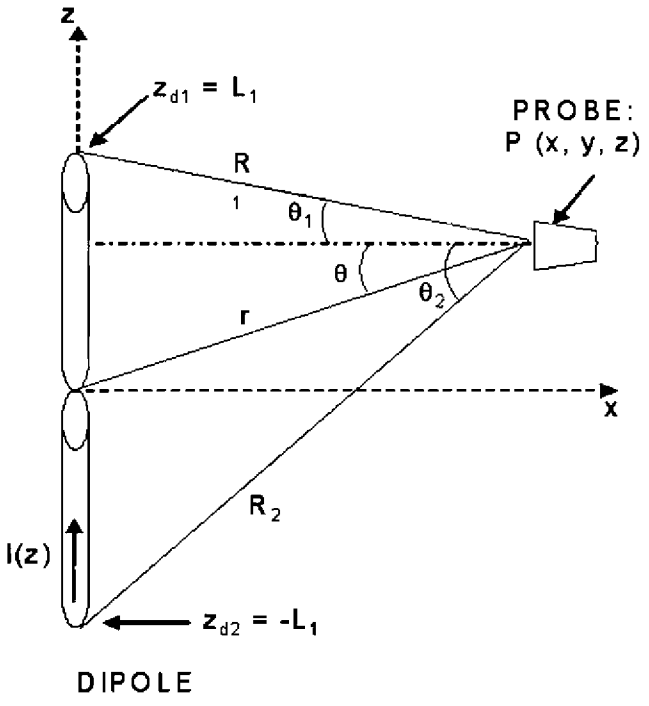

Figure 2 Geometry of the dipole and probe.

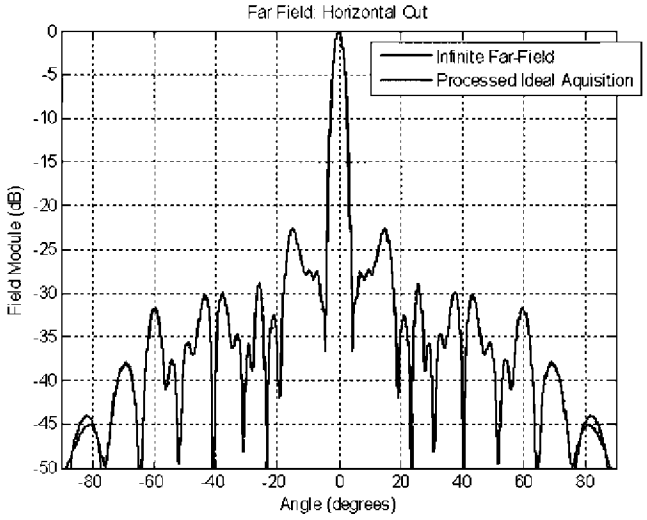

Figure 3 Horizontal cut: Infinite far-field versus processed ideal acquisition

This tool is also useful for testing the elevation validity range of the NF-FF transformation. This range is often approximated by the method proposed by Yaghjian and Newell :

$$\theta_0 = \tan^{-1}\frac{L_z - D_z}{2x_o} \tag{9}$$

With this configuration of the cylindrical system and the modeling of the AUT, the angular range of validity goes from 37.8° to 142.2°.

Figure 4 confirms that the angular margin of the measurement is valid. In addition, the cylindrical NF-FF transformation software was also validated through measurements in a spherical near-field system that were performed in the antenna test facility of the Technical University of Madrid (LEHA-UPM, Antenna Homologation and Test Facility), using the SNIFTD transformation Software The validation through intercomparisons was carried out with a Ku-reflector—shown in Figure 5—and a $\mu = \pm 1$ probe and comparing the results achieved in the cylindrical system with the ones attained in the spherical range. The results of this inter-

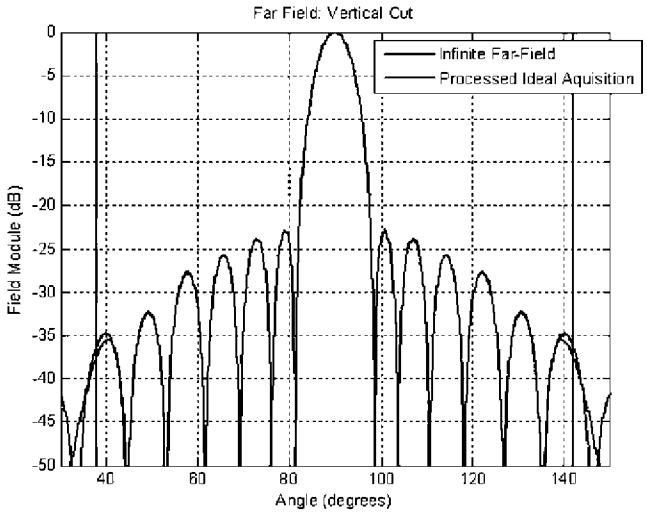

Figure 4 Vertical cut: Infinite far-field versus processed ideal acquisition

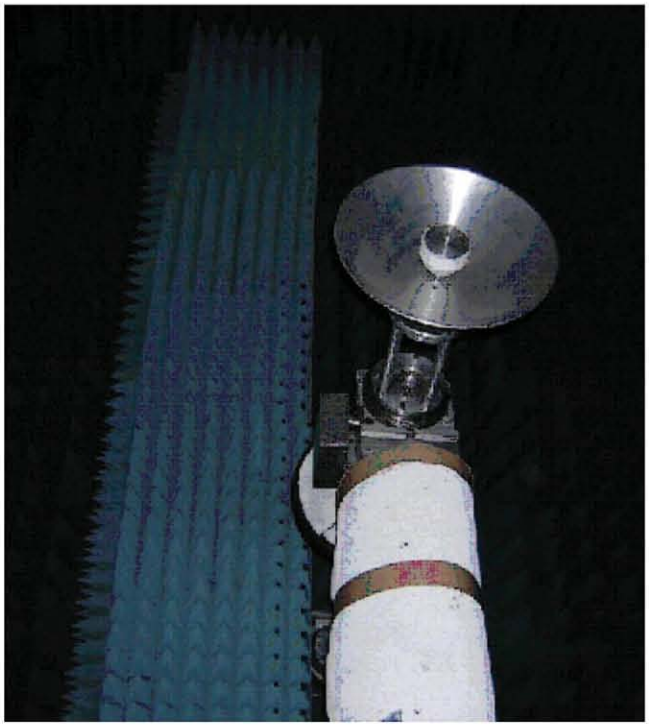

Figure 5 Ku reflector employed for the intercomparisons.

comparison process are illustrated in Figures 6 and 7. From these graphs, a very good agreement is observed in both planes in either vertical or horizontal pattern, also showing the angular margin of the measurement (straight vertical lines).

4. APPLICATION

Apart from the system validation, an exhaustive evaluation of the measurement system was carried out. The main specifications of the measurement system used for this evaluation are fully detailed

In this case, the frequency range selected was the L-band, from 1000 to 1400 MHz.

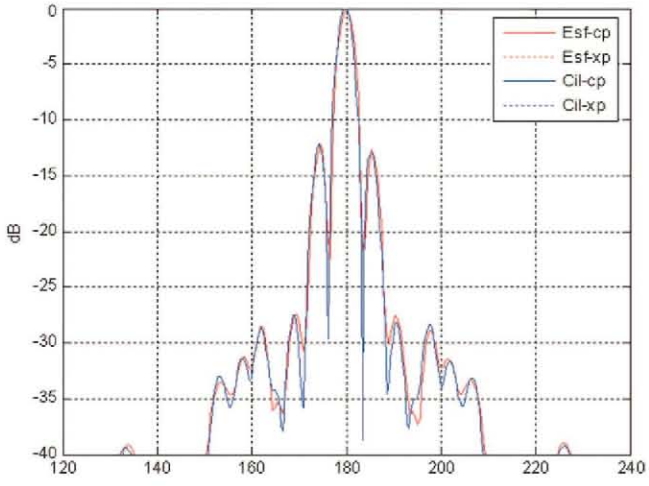

Figure 6 Horizontal cut for the measurement with the Ku-reflector.

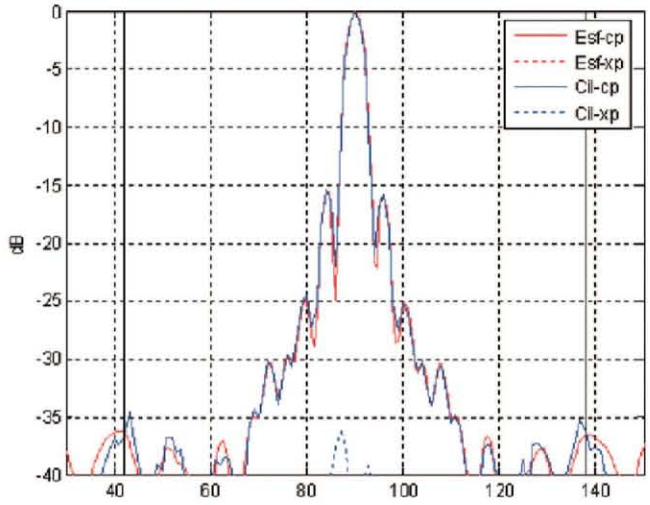

Figure 7 Vertical cut for the measurement with the Ku-reflector.

The general specifications establish that the AUT could be up to 12-m long, up to 7.5-m high and that the linear slide has a maximum length of only 15.5 m. Furthermore, the distance from the AUT to the probe can vary form 5 up to 7 m, and the azimuth angular range covers from 0° to 360°. In addition, the minimum rotation velocity of the AUT, that is, the velocity for the measurement process, goes from 5 to 7.5 rpm. In this case, the antenna considered was smaller (5.3 m × 2.1 m), and the separation distance between the antennas was set to 5 m. Figure 8 shows an example of the system implementation.

To finish this study, an evaluation of the measurement system was carried out by means of the measurements done in the cylindrical outdoor facility. Figure 9 represents the radiation pattern achieved after processing the measurements of a L-band RADAR antenna, which has a sum diagram in the horizontal cut and a

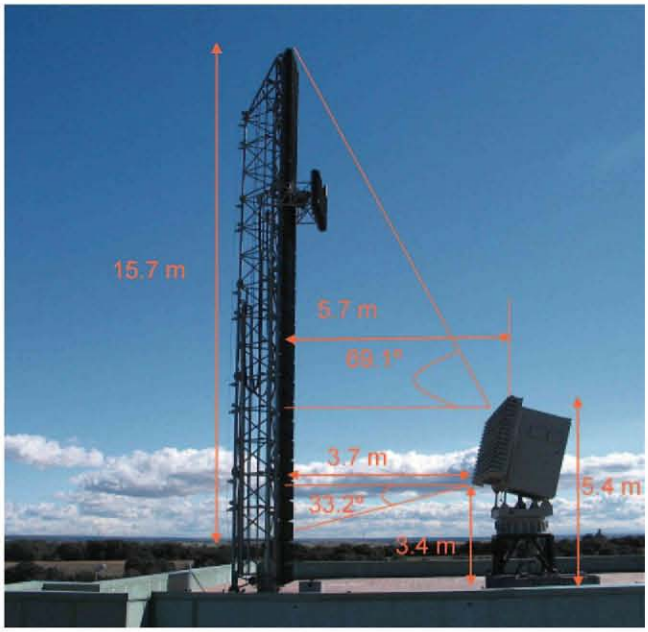

Figure 8 System implementation.

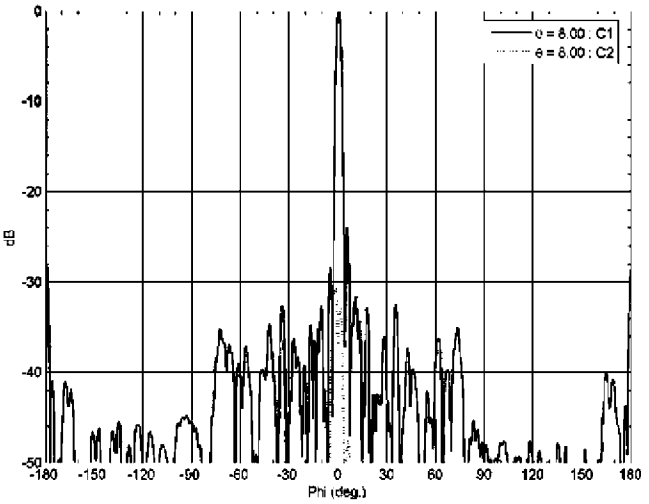

Figure 9 Measured horizontal radiation pattern.

difference diagram in the vertical plane. The figure illustrates the horizontal cut of the far-field radiation pattern measured. From this graph, it could be noticed that although there are some reflections in the back direction coming from a fence, the error requirements indicated in the system specifications are satisfied; the maximum error in gain is of the order of ± 0.5 dB, the error at -30 dB of SLL is ± 2 dB, the error at -40 dB of SLL $\pm$ 3 dB, and the pointing error is $\pm 0.05^\circ$ in azimuth and $\pm 0.1^\circ$ in elevation planes.

5. CONCLUSION

An algorithm to perform the cylindrical NF-FF transformation has been developed and validated. The validation has been carried out through simulations and intercomparisons. The simulator to evaluate the algorithm models the AUT, using vertical dipoles over an infinite ground plane. The virtual acquisition has been performed simulating an ideal conical horn moving vertically on the generatrix of a cylinder and rotating in azimuth the AUT. Besides, the cylindrical modes of the antenna probe were obtained through the evaluation of the copolar component of the two main planes (E and H plane), as it is usually done in spherical NF-FF algorithms. These modes are used for the probe correction algorithm. The simulator was used in the design phase of the L-band RADAR antenna measurement system, and nowadays, the authors are using this simulator to analyze the influence of mechanical and electrical errors in the measurement errors and uncertainties.

Furthermore, the cylindrical NF-FF acquisition and transformation has been compared with the SNIFTD on a Ku-band reflector antenna, showing accurate results. Finally, this algorithm has been used on a very large L-band RADAR antenna, performing the acquisition on a huge grid: 512 samples in azimuth times 156 samples in z-axis with large radial distances (up to 7 m) in a cylindrical outdoor range, obtaining a radiation pattern similar to the designed one.

REFERENCES

J. Romeu, M. Baquero, M. Ferrando, L. Jofre, J. Alemany, V. González, "A cylindrical near field test facility," Microwave Eng Europe (1990), 25–31.

G.V. Borgiotti, "Integral equation formulation for probe corrected far-field reconstruction from measurements on a cylinder," IEEE Trans Antennas Propag AP-26 (1978), 572–578.

J.A. Hansen, "On cylindrical near-field scanning techniques," IEEE Trans Antennas Propag AP-28 (1980), 231–234.

A.D. Yaghjian, An overview of near-field antenna measurements," IEEE Trans Antennas Propag AP-34 (1986), 30–45.

W. Rudge, K. Milne, A.D. Olver, and P. Knight, The handbook of antenna design, Vol. 1, 1982, pp. 609–614.

J. Brown and E.V. Jull, "The prediction of aerial radiation patterns from near-field measurements," Inst Elec. Eng. Pap 3649E (1961).

W.M. Leach, Jr. and D.T. Paris, "Probe compensated near field measurements on a cylinder," IEEE Trans Antennas Propag 214 (1973), 435–445.

O.M. Bucci, "Use of sampling expansions in near-field-far-field transformations: The cylindrical case," IEEE Trans Antennas Propag 36 (1988), 830–835.

Z.A. Hussein and Y. Rahmat-Samii, "Probe compensation characterization in cylindrical near-field scanning," IEEE (1993), 1808–1811.

P. Petre and T.K. Sarkar, "Planar near-field to far-field transformation using an equivalent magnetic current approach," IEEE Trans Antennas Propag 40 (1992), 1348–1356.

T.K. Sarkar and A. Taaghol, "Near-field to near/far-field transformation for aribitrary near-field geometry utilizing an equivalent electric current and MoM antennas and propagation," IEEE Trans Antennas Propag 47 (1999), 566–573.

S. Blanch, L. Jofre, and J. Romeu, "Comparision between classical and equivalent current approach near-field to far-field transformation," Antenna Propag Soc Int Symp Dig 1 (1995), 260–263.

F.L. Heras, B. Galocha, and J.L. Besada, "Far-field performance of linear antennas determined from near-field data," IEEE Trans Antennas Propag 50 (2002), 408–410.

F.L. Heras, B. Galocha, and J.L. Besada, "Circular scanning and equivalent magnetic currents for main plane near-field transformation," Int J Numer Model: Electron Networks, Dev Fields 15 (2005), 329–338.

Y. Rahmat-Samii, "Useful coordinate transformations for antenna applications," IEEE Trans Antennas Propag 27 (1979), 571–574.

R.S. Elliot (Ed.), "Antenna theory and design," Prentice-Hall, Englewood Cliffs, NJ.

A.D. Yaghjian, "Upper-bound errors in far-field antenna parameters determined from planar near-field measurements, Part 1: Analysis," Nat Bur Stand Tech Note 667 (1975).

A.C. Newell and M.L. Crawford, "Planar near-field measurements on high performance array antennas," Nat Bur Stand NBSIR 74–380 (1974).

Homepage of SNIFTD. http://www.ticra.com/script/site/page.asp?artid=27.

F. Martín, S. Burgos, M. Sierra-Castañer, and J.L. Besada, "Design of a cylindrical near field system for RADAR antennas," EuCAP symposium proceedings, Nice, France, November 2006.